

Testing redMaPPer Centring Probabilities using Galaxy Clustering and Galaxy-Galaxy Lensing

Chiaki Hikage¹, Rachel Mandelbaum², Alexie Leauthaud^{3,1}, Eduardo Rozo⁴, Eli S. Rykoff^{5,6}

¹ *Kavli Institute for the Physics and Mathematics of the Universe (Kavli IPMU, WPI), University of Tokyo, 5-1-5 Kashiwanoha, Kashiwa, Chiba, 277-8583, Japan*

² *McWilliams Center for Cosmology, Department of Physics, Carnegie Mellon University, Pittsburgh, PA 15213, USA*

³ *Department of Astronomy and Astrophysics, University of California Santa Cruz, Santa Cruz, CA 95064, USA*

⁴ *Department of Physics, University of Arizona, Tucson, AZ 85721, USA*

⁵ *Kavli Institute for Particle Astrophysics & Cosmology, P. O. Box 2450, Stanford University, Stanford, CA 94305, USA*

⁶ *SLAC National Accelerator Laboratory, Menlo Park, CA 94025, USA*

7 September 2018

ABSTRACT

Galaxy cluster centring is a key issue for precision cosmology studies using galaxy surveys. Mis-identification of central galaxies causes systematics in various studies such as cluster lensing, satellite kinematics, and galaxy clustering. The red-sequence Matched-filter Probabilistic Percolation (redMaPPer) estimates the probability that each member galaxy is central from photometric information rather than specifying one central galaxy. The redMaPPer estimates can be used for calibrating the off-centring effect, however, the centring algorithm has not previously been well-tested. We test the centring probabilities of redMaPPer cluster catalog using the projected cross correlation between redMaPPer clusters with photometric red galaxies and galaxy-galaxy lensing. We focus on the subsample of redMaPPer clusters in which the redMaPPer central galaxies (RMCGs) are not the brightest member galaxies (BMEM) and both of them have spectroscopic redshift. This subsample represents nearly 10% of the whole cluster sample. We find a clear difference in the cross-correlation measurements between RMCGs and BMEMs, and the estimated centring probability is $74 \pm 10\%$ for RMCGs and $13 \pm 4\%$ for BMEMs in the Gaussian offset model and $78 \pm 9\%$ for RMCGs and $5 \pm 5\%$ for BMEMs in the NFW offset model. These values are in agreement with the centring probability values reported by redMaPPer (75% for RMCG and 10% for BMEMs) within 1σ . Our analysis provides a strong consistency test of the redMaPPer centring probabilities. Our results suggest that redMaPPer centring probabilities are reliably estimated. We confirm that the brightest galaxy in the cluster is not always the central galaxy as has been shown in previous works.

Key words: galaxies: clusters: general

1 INTRODUCTION

In the standard hierarchical structure formation scenario, small dark matter haloes form first and grow by accretion of surrounding matter and also by merging other haloes. When a small halo merges into a more massive halo, the galaxy that was originally the central galaxy in the small halo becomes a satellite galaxy in the merged halo, while the central galaxy hosted by the more massive halo remains the central galaxy of the final dark matter halo. After merging, the star formation of satellite galaxies is quenched. The central galaxy continues to accrete new gas from satellite galaxies. In consequence, the central galaxy is luminous, massive, and is located near the bottom of the halo potential well. Actually central galaxies form distinct population from other smaller neighboring galaxies, i.e., satellites, in many aspects such as color, star formation activity, AGN activity, morphology, and

stellar populations (Weinmann et al. 2006; von der Linden et al. 2007; van den Bosch et al. 2008; Skibba 2009; Hansen et al. 2009).

We define the central galaxy as the one with the lowest specific potential energy in each cluster. Identifying central galaxies in galaxy groups and clusters is important for both cosmology and galaxy evolution studies. Off-centred clusters that are used in stacked lensing analysis without any modeling to account for the off-centring cause systematics in the mass estimation (Johnston et al. 2007; Leauthaud et al. 2010; Okabe et al. 2010; Oguri & Takada 2011; George et al. 2012; Hikage et al. 2013). The clustering properties of central and satellite galaxies are different and this features in the commonly used halo occupation modeling (HOD: Seljak 2000; Scoccimarro et al. 2001; Berlind & Weinberg 2002; Zheng et al. 2005; Masjedi et al. 2006; Reid & Spergel 2009; White et al. 2011; Leauthaud et al. 2011; Coupon et al. 2012; Manera et al. 2013; Parejko et al. 2013). Inter-

nal motions of satellite galaxies generate the non-linear redshift-space distortion, which is a systematic uncertainty in cosmology studies from redshift-space galaxy clustering (Cabr e & Gazta ana 2009; Reid et al. 2009; Samushia et al. 2012; Hikage et al. 2012; Hikage & Yamamoto 2013; Guo et al. 2015). In the studies of satellite kinematics, off-centred galaxies lead to overestimate halo masses (Skibba et al. 2011).

Identifying central galaxies are not always simple unless there is a dominant cD galaxy at the X-ray peak emission. The central galaxy is often assumed to be the brightest galaxy in the cluster (BCG) (van den Bosch et al. 2004; Weinmann et al. 2006; Budzynski et al. 2012). There are, however, many studies indicating that a significant fraction of central galaxies are not BCGs (van den Bosch et al. 2005; von der Linden et al. 2007; Coziol et al. 2009; Sanderson et al. 2009; Einasto et al. 2011; Skibba et al. 2011; George et al. 2012; Hikage et al. 2013; Sehgal et al. 2013; Lauer et al. 2014; Hoshino et al. 2015). For example, Skibba et al. (2011) use phase-space statistics to find that the off-centring fraction, i.e., the fraction of BCGs that are not the central galaxy, increases from $\sim 25\%$ for Milky-Way size halos to $\sim 45\%$ for massive clusters. Hikage et al. (2013) use the redshift-space power spectrum, galaxy-galaxy lensing, and the cross-correlation with photometric galaxies, and found that the off-centring fraction for massive clusters is $46\pm 5\%$. Lauer et al. (2014) use nearby clusters to find that $\sim 15\%$ of BCGs have large offsets ($> 100\text{kpc}$) from X-ray centres. While high-resolution X-ray and SZ data can help robustly identify the deepest part of the cluster potential well and therefore the true cluster central galaxy (e.g., Ho et al. 2009; George et al. 2012; Stott et al. 2012; von der Linden et al. 2014; Menanteau et al. 2013; Mahdavi et al. 2013; Rozo & Rykoff 2014; Oguri 2014), the size of the cluster sample with the necessary data is quite limited.

The red-sequence Matched-filter Probabilistic Percolation (redMaPPer) is a red-sequence cluster finding algorithm (Rykoff et al. 2014; Rozo & Rykoff 2014), which is optimized for multi-band photometric surveys such as the Sloan Digital Sky Survey (SDSS; York et al. 2000), the Hyper-Suprime Cam (HSC; Miyazaki et al. 2012) survey, the Dark Energy Survey (DES; The Dark Energy Survey Collaboration 2005), and the Large Synoptic Survey Telescope (LSST; Ivezi c et al. 2008). A similar red-sequence based cluster finding algorithm called CAMIRA (Cluster finding Algorithm based on Multi-band Identification of Red-sequence gAlaxies) has also been developed to provide a cluster catalog using Hyper-Suprime Cam data in a wide range of redshifts (Oguri 2014; Oguri et al. 2017). A key feature of the redMaPPer algorithm is that it estimates the centring probability of every member galaxy rather than identifying from three photometric observables: luminosity, color, and the local galaxy density. redMaPPer estimates of centring probabilities are useful for calibrating the systematics associated with the off-centring effect in various cosmology studies such as cluster mass estimates using stacked lensing analysis and satellite kinematics and also the accurate modeling of the redshift-space clustering. However, there was not enough verification of the redMaPPer centring probabilities. Hoshino et al. (2015) found that the off-centring probability of the brightest cluster member galaxy is 20-30% using the redMaPPer centring probability, while Skibba et al. (2011) found that the off-centring value is 40% using phase-space statistics. The results in Hoshino et al. (2015) rely on the assumption that the redMaPPer central probability is accurate. Validating that result and many other cosmological studies using the redMaPPer algorithm requires us to verify that the redMaPPer centring probability

is an accurate reflection of reality. The accuracy of the redMaPPer centring probability was previously studied by comparison with X-ray clusters (Roza & Rykoff 2014). The overlapped area for the comparison is small and thus the result depends on the selected X-ray subsamples.

Cluster-galaxy lensing, a cross-correlation of foreground clusters with background galaxy shapes, provides an estimate of the projected mass distribution around the foreground clusters (e.g., Mandelbaum et al. 2006; Sheldon et al. 2009; Leauthaud et al. 2010; Okabe et al. 2010; Mandelbaum et al. 2013). When the lens sample contains off-centred (satellite) galaxies, the stacked lensing signals are modified in a way that depends on the satellite fraction and radial offsets (Johnston et al. 2007; Leauthaud et al. 2010; Okabe et al. 2010; Oguri & Takada 2011; George et al. 2012; Hikage et al. 2013). The cross-correlation with photometric galaxies provides another way to evaluate the central fraction of a given galaxy sample statistically (Mandelbaum et al. 2013; Hikage et al. 2013).

In this paper, we test the redMaPPer centring probability using the cross-correlation measurements, and verify the results using cluster-galaxy lensing. Here we focus on the clusters for which the brightest member galaxy does not have the highest central galaxy probability according to the redMaPPer algorithm. These clusters usually do not have well-defined central galaxies, and therefore provide a good sample to check whether the redMaPPer centring probability agrees with the estimation from the cross-correlation measurements. We also select a sample with highly secure central galaxy identification as a reference sample.

This paper is organized as follows: in section 2 we describe the details of the galaxy cluster sample. In section 3 we explain how to estimate cross-correlation with the photometric red galaxies and galaxy-galaxy lensing. In section 4, the theoretical model to compare with the observations to estimate the off-centring properties is described. In section 5, we present the results of the cross-correlation measurements with different proxies of central galaxies and constraints on their central fraction. Section 6 is devoted to summary and conclusions. Throughout this paper, we adopt a flat Λ cold dark matter cosmology with $\Omega_m = 0.3$ and $\sigma_8 = 0.8$. We use physical (not comoving) units for distances and lensing signals.

2 DATA

2.1 Galaxy cluster samples

redMaPPer is a red-sequence cluster finding algorithm (see the details of the algorithms in Rykoff et al. 2014; Roza & Rykoff 2014). It utilizes the 5-band (*ugriz*) imaging data to identify galaxy clusters by characterizing the evolution of red sequence in an iterative self-training technique. redMaPPer estimates the photometric redshift of each cluster z_λ and the cluster richness λ from the membership probability assigned to each galaxy in a cluster field (Roza et al. 2015). Our sample is constructed from the redMaPPer v5.10 cluster catalog (Roza et al. 2015) based on the Sloan Digital Sky Survey Data Release 8 (SDSS DR8) photometric data (Aihara et al. 2011). The sample covers about $10,000 \text{ deg}^2$ contiguous sky area with the same survey mask of Baryon Oscillation Spectroscopic Survey (BOSS; Dawson et al. 2013). We extract a sample of 7730 redMaPPer galaxy clusters with $\lambda \geq 20$ in the range $0.16 < z_\lambda < 0.33$, which is identical to the sample analyzed by (Hoshino et al. 2015). We impose an additional mask for the cross-correlation and lensing measurements to

match the area coverage of the fainter sample used for these cross-correlations (see the details in Reyes et al. 2012; Nakajima et al. 2012; Mandelbaum et al. 2012, 2013)

A key feature of redMaPPer is that it assigns a centring probability P_{cen} to every member galaxy. When there is a well-defined central galaxy, the P_{cen} of the galaxy approaches unity. Otherwise P_{cen} may be well below unity. The centring probability P_{cen} of every member galaxy candidate is estimated from three filters:

$$u_{\text{cen}} = \phi_{\text{cen}}(m_i|z_\lambda, \lambda)G_{\text{cen}}(z_{\text{red}})f_{\text{cen}}(w|z_\lambda, \lambda), \quad (1)$$

where the luminosity filter ϕ_{cen} uses the i -band magnitude m_i , the photometric redshift (color) filter G_{cen} uses the photometric redshift z_{red} , and the local density filter f_{cen} depends on the gravitational potential weight w . A higher value is returned for galaxies where the luminosity is higher in ϕ_{cen} , the photometric redshift is closer to the cluster redshift in G_{cen} , and the local density is higher in f_{cen} . Each filter is assumed to be a Gaussian distribution with both its mean and its dispersion in ϕ_{cen} and f_{cen} dependent on z_λ and λ . The dispersion of z_{red} in G_{cen} is set to be broad so that the galaxies that have slightly offset colors are allowed to be central galaxies. Since the redMaPPer centring probability depends on the above three observables, the brightest member galaxy (hereafter denoted by BMEM) does not always have the highest centring probability when the galaxy is isolated from other galaxies. In this paper, we call the galaxy with the highest centring probability “redMaPPer central galaxy” (hereafter denoted by RMCG).

We focus on clusters for which the RMCG and BMEM are not the same. Since these clusters usually lack a well-defined central galaxy, they are particularly useful for testing whether the redMaPPer centring probability is correct. An example of such clusters is shown in Fig.6 of our previous paper (Hoshino et al. 2015). In order to reduce contamination from projection effects, we further restrict the sample to the clusters for which both the RMCGs and BMEMs have confirmed spectroscopic redshifts in the BOSS LOWZ DR12 sample (Alam et al. 2015) and their redshifts are consistent within 3σ , i.e., $|z^{\text{RMCG}} - z^{\text{BMEM}}|/(1 + z^{\text{RMCG}}) < 3\sigma_v$, where c is the speed of light and σ_v is the velocity dispersion inside clusters. We adopt a richness- and redshift-dependent σ_v in the form of $\sigma_v = \sigma_p((1 + z_\lambda)/(1 + z_p))^\beta(\lambda/\lambda_p)^\alpha$ with the best-fitting value of $\sigma_p = 618.1$ km/s, $z_p = 0.171$, $\lambda_p = 33.336$, $\alpha = 0.435$, $\beta = 0.54$ fitted to the redMaPPer clusters (Rozo et al. 2015). The final number of galaxy clusters is reduced to 743, which is 9.6% of the total cluster sample in the same range of z_λ and λ . The average richness and redshift of this sample is $\langle\lambda\rangle = 36.1$ and $\langle z_\lambda\rangle = 0.253$. The mean centring probability values that are reported by redMaPPer for this sample are 0.754 for RMCGs and 0.103 for BMEMs. The distributions of z_λ , λ and P_{cen} for RMCG and BMEM samples are plotted in Figure 1. The distributions are normalized to the total number of galaxy clusters in the sample.

As a reference sample of central galaxies, we construct a “High Pcen” sample for which the centring probability of RMCGs is larger than 99% and for which the RMCG has a spectroscopic redshift that is consistent with the spectroscopic redshift of at least one other cluster member. The number of galaxies in the “High Pcen” sample is 1385 and its average $\langle\lambda\rangle = 37.3$ and $\langle z_\lambda\rangle = 0.251$, consistent with the RMCG/BMEM samples. The distributions of z_λ and λ for the High Pcen sample are also plotted in Figure 1.

In summary, we prepare three “central galaxy” samples:

(i) RMCG: clusters with different RMCG and BMEM, and the centre defined as RMCG

(ii) BMEM: clusters with different RMCG and BMEM, and the centre defined as BMEM

(iii) High Pcen: clusters with the centring probability of RMCG is higher than 99%

We remake random catalogs to match the distribution of λ and z_λ in each sample, and the same sky coverage as the whole cluster catalog.

3 MEASUREMENTS

3.1 Projected cross-correlation of galaxy clusters with photometric red galaxies

In order to constrain the off-centring fraction in each “central galaxy” sample described in the previous section, we use the projected cross-correlation function of each central galaxy with a sample of photometric red galaxies selected from the source catalog from SDSS DR8. The spectral energy distribution (SED) and photo- z are estimated with the Zurich Extragalactic Bayesian Redshift Analyzer (ZEBRA; Feldmann et al. 2006). We use red galaxies by selecting those galaxies for which the ZEBRA results are consistent with an early-type galaxy SED, and a cut is imposed on the extinction-corrected model magnitude at $r < 21$ to restrict to a sample with smaller photometric redshift errors. Systematic tests of the redshifts for this photometric sample were carried out in Nakajima et al. (2012).

The projected cross-correlation function for each central galaxy sample (RMCG, BMEM, or High Pcen) is estimated as follows:

$$w^{\text{cross}}(R) = \frac{D^{(\text{cluster})}D^{(\text{photo}-z)}}{R^{(\text{cluster})}D^{(\text{photo}-z)}} - 1, \quad (2)$$

where $D^{(\text{cluster})}D^{(\text{photo}-z)}$ is the number of pairs between cluster central galaxies and photo- z galaxies at the projected separation of R (calculated at the cluster redshift). For this purpose, we only use pairs for which the photo- z is consistent with the cluster redshift within 1σ and the number is normalized with the total number of pairs. $R^{(\text{cluster})}D^{(\text{photo}-z)}$ is same as $D^{(\text{cluster})}D^{\text{photo}-z}$ but for the number of pairs between a random catalog corresponding to the cluster distributions and photo- z galaxies. The amplitude of the cross-correlation depends on the photo- z error because the photo- z galaxies that are not physically associated with the galaxy clusters dilute the cross-correlation signal. As a result, we marginalize over the amplitude information in our analysis.

The covariance matrix for the projected clustering signal, and the cross-covariance between different samples, is estimated using the jackknife resampling method, which for clustering seems to overestimate the covariance by about 10% on scales below the jackknife region size (Singh et al. 2017). The scales that dominate our constraints all satisfy this requirement.

3.2 Galaxy-galaxy lensing

We also use the galaxy-galaxy lensing, the cross-correlation of each central galaxy with shapes of background galaxies. Since this measurement is directly sensitive to the matter distribution around the lens galaxies, it is also a useful probe of off-centring of these galaxies within their host halos. The galaxy-galaxy lensing measurement, however, has a larger statistical error compared to the cross-correlation measurements and is primarily used for a consistency check.

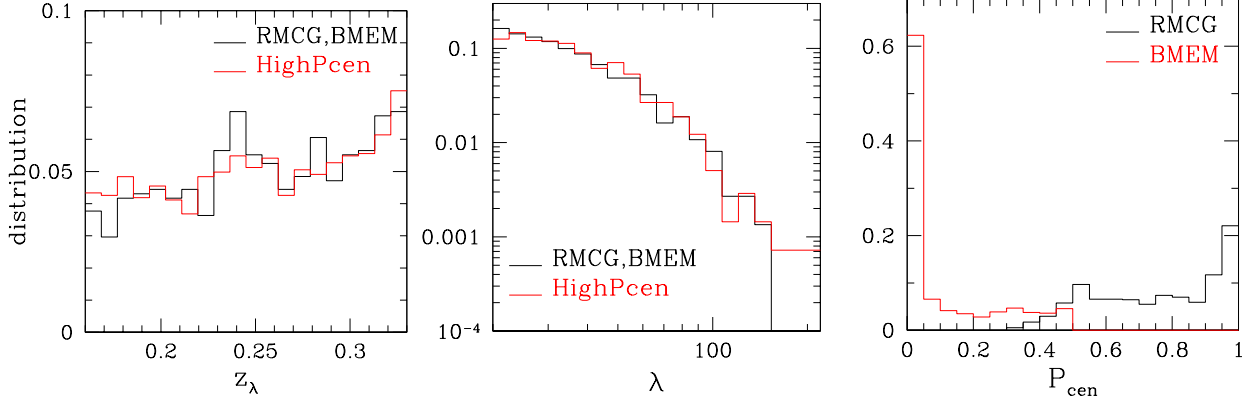


Figure 1. Histograms of photometric redshift z_λ (left) and richness λ (middle) for redMaPPer central galaxies (RMCG), brightest member galaxies (BMEM) and High Pcen sample, which is the reference sample of ‘central’ galaxies with the redMaPPer centring probability higher than 99%. The details of the samples are written in the text. The distributions of both z_λ and λ are similar among the samples. The right panel shows the P_{cen} distribution for the RMCG and BMEM samples. The histogram is normalized by the total number of galaxy clusters in each sample. Since the RMCG and BMEM samples are specifically chosen to include clusters for which the RMCG and BMEM galaxy are not the same, the redMaPPer centring probability of BMEMs is much lower than that of RMCGs. This is not the case when considering all redMaPPer clusters.

The source galaxy sample is selected from the same source catalog as described above. The source galaxy shapes are measured with the re-Gaussianization method (Hirata & Seljak 2003). We use a shear catalog with a number density of 1.2 per square arcmin, which was first presented in Reyes et al. (2012) and further tested and validated in later work (Nakajima et al. 2012; Mandelbaum et al. 2012, 2013). For the lensing measurement, we use source galaxies to the faint limit of the catalog (extinction-corrected model magnitude $r < 21.8$) with photometric redshift larger than each central galaxy. Galaxy-galaxy lensing is measured with the differential projected mass density $\Delta\Sigma(R)$, which is optimally estimated as (Mandelbaum et al. 2006)

$$\Delta\Sigma(R) = \frac{\sum_{\text{ls}} w_{\text{ls}} \gamma_t^{(\text{ls})}(R) \Sigma_{\text{crit}}(z_l, z_s)}{\sum_{\text{rs}} w_{\text{rs}}} - \frac{\sum_{\text{rs}} w_{\text{rs}} \gamma_t^{(\text{rs})}(R) \Sigma_{\text{crit}}(z_r, z_s)}{\sum_{\text{rs}} w_{\text{rs}}}, \quad (3)$$

where γ_t is the tangential shear with respect to each lens galaxy and Σ_{crit} is the critical surface mass density given as

$$\Sigma_{\text{crit}}(z_l, z_s) = \frac{c^2}{4\pi G} \frac{D_A(z_s)}{D_A(z_l) D_A(z_l, z_s)}, \quad (4)$$

with the angular diameter distance $D_A(z)$. The subtraction of tangential shear around random points removes contributions from additive systematics and results in a more optimal estimator (Singh et al. 2017). The division by the sum of weights around random points accounts for the dilution of the signal by unlensed cluster member galaxies that are included in the source sample due to photo- z error (Mandelbaum et al. 2005). The shear weight for galaxies and random, w_{ls} and w_{rs} respectively, is given as the inverse variance weight

$$w = \Sigma_{\text{crit}}^{-2}(z_l, z_s) (\sigma_{\text{int}}^2 + \sigma_i^2), \quad (5)$$

where σ_{int} is the intrinsic ellipticity fixed to be 0.365 and σ_i is the shape measurement error due to pixel noise (Reyes et al. 2012).

As illustrated in Singh et al. (2017), for g-g lensing, the jackknife method properly represents the covariance below the jackknife region size. This validates our choice of jackknife errorbars.

4 THEORETICAL MODELING

In this section, we provide a theoretical modeling of the projected cross-correlation $w(R)$ and galaxy-galaxy lensing $\Delta\Sigma(R)$ based on the previous work by Hikage et al. (2013).

In order to take into account the halo mass dependence of the radial profile of photo- z galaxies, we convert the richness distribution of the clusters $P(\lambda)$ to the halo mass distribution $P(M)$ by

$$P(M) = \int d\lambda P(\lambda) P(M|\lambda), \quad (6)$$

where $P(M|\lambda)$ is the conditional mass distribution for a fixed λ . Here we use $P(M|\lambda)$ calibrated by the galaxy-galaxy lensing analysis of Simet et al. (2017). They model $P(M|\lambda)$ as a lognormal distribution with a mean mass-richness relation that is parametrized as

$$\langle M|\lambda \rangle = M_0 \left(\frac{\lambda}{\lambda_0} \right)^\alpha, \quad (7)$$

where the pivot scale of richness λ_0 and α is the power-law slope of a mass at a given λ . The scatter in mass at a fixed richness is given as the sum of a Poisson term and an intrinsic variance term as

$$\text{Var}(\ln M|\lambda) = \frac{\alpha^2}{\lambda} + \sigma_{\ln M|\lambda}^2. \quad (8)$$

The halo mass M is defined as M_{200m} , the mass enclosed in a sphere of 200 times the mean matter density. We use their best-fit values $\log(M_0/h^{-1}M_\odot) = 14.344$ at $\lambda_0 = 40$, and $\alpha = 1.33$. The variance $\sigma_{\ln M|\lambda}$ is set to be 0.25. The mean mass $\log(M/h^{-1}M_\odot)$ is 14.3 for both of our RMCG/BMEM and High Pcen samples.

We employ the Navarro-Frenk-White (NFW) profile (Navarro et al. 1996) to describe the distribution of the red galaxies inside halos by replacing the mass with the galaxy number:

$$\rho_g(r) = \frac{\rho_{g,s}}{(r/r_s)(1+r/r_s)^2}, \quad (9)$$

where the density parameter $\rho_{g,s}$ is given by

$$\rho_{g,s} = \frac{N_g(M)}{4\pi r_s^3 (\log(1+c) - c/(1+c))}. \quad (10)$$

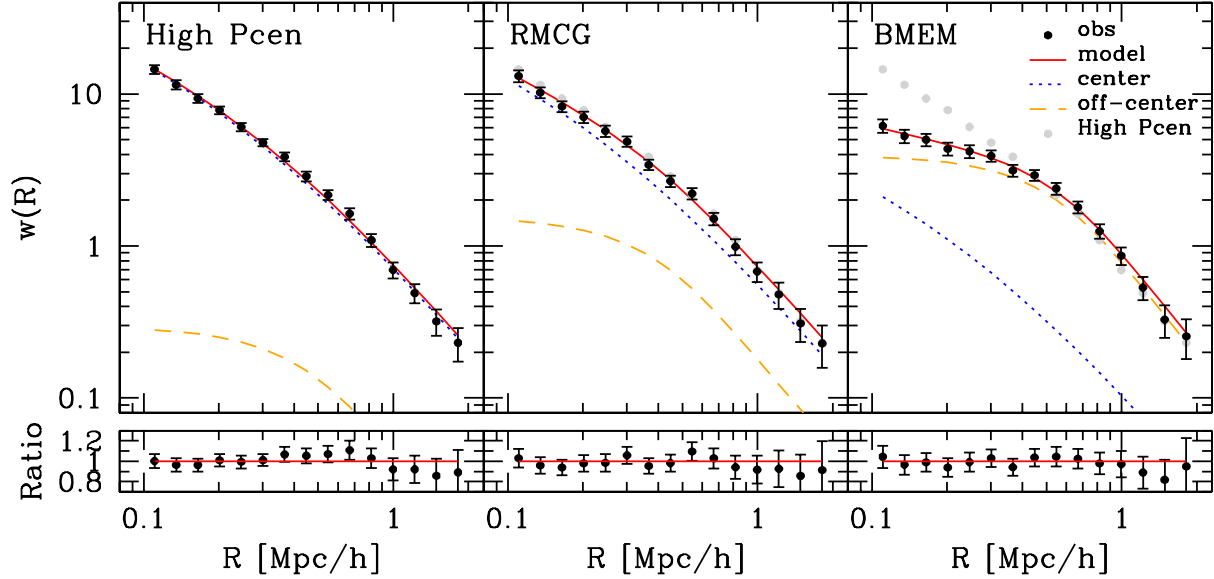


Figure 2. Cross-correlation measurements of photometric red galaxies with High Pcen galaxies (left), redMaPPer central galaxies (middle) and brightest galaxy samples (right) are shown as black filled circles. Data points for the High Pcen sample are plotted in the right two panels with thin gray points for reference. We also plot the best-fitting model (Eq. 13, red solid lines); centring and off-centring components are plotted with blue dotted and yellow dashed lines respectively. The error is estimated from jackknife resampling. As shown, the clustering of red galaxies around RMCGs is close to be that of red galaxies around High Pcen sample, and the profile is much steeper than that of red galaxies around BMEMs. This indicates that the centring fraction of RMCGs is much larger than BMEMs. Lower panels show the ratio of observed values to the best-fitting model.

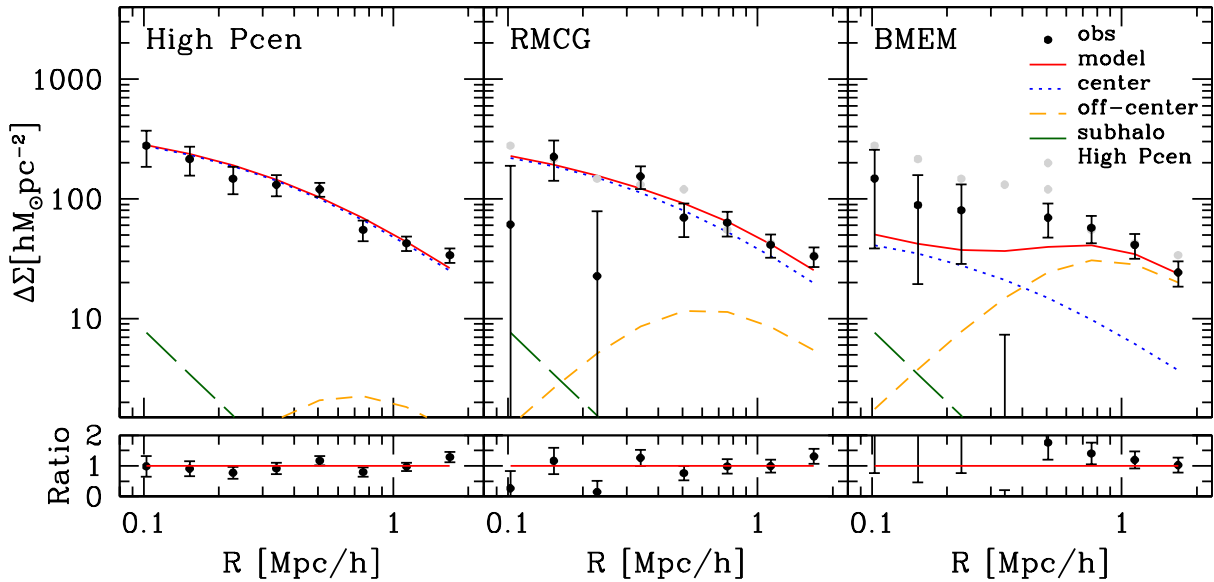


Figure 3. Same as Fig. 2 but for the galaxy-galaxy lensing $\Delta\Sigma$. We use the model in Equation (15) with the best-fitting values of q_{cen} and τ_{off} obtained from the cross-correlation $w(R)$. We set $\log(M_*/h^{-1}M_\odot) = 11.4$. While the lensing data are too noisy to fit a new model, this figure demonstrates that the lensing data are consistent with the model derived from the cross-correlation measurements.

The value of $N_g(M)$ represents the number of photo- z galaxies inside a halo with the mass of M assuming that $N_g(M)$ is proportional to M as

$$N_g(M) = \frac{M \rho_g(z)}{\rho_m(z)}, \quad (11)$$

where $\rho_m(z)$ and $\rho_g(z)$ are the average mass density and the average number density of photo- z galaxies at redshift z . Here the halo mass is defined as M_{200m}

$$M \equiv \frac{4\pi r_{200m}^3}{3} \cdot 200 \rho_m(z), \quad (12)$$

where r_{200m} is the radius corresponding to M_{200m} and then the concentration is defined as $c \equiv r_{200m}/r_s$. We adopt the mass-concentration relation from Diemer & Kravtsov (2015). The amplitude of the mass-concentration relation is left as a free parameter – i.e., the overall amplitude of that relation is multiplied by a mass-independent factor c_{amp} . We describe the projected cross-correlation function $w(R)$ by adding an off-centring term to model “central” galaxies that are offset from halo centres as:

$$w(R) = \int \frac{k dk}{2\pi} C_{\text{gg}}(k) J_0(kR), \quad (13)$$

and

$$C_{\text{gg}}(k) = \frac{1}{\Delta\chi} \int dM P(M) \left(\frac{N_g(M)}{\rho_g(z)} \right) \tilde{u}_{\text{NFW}}(k; M) \times [q_{\text{cen}} + (1 - q_{\text{cen}}) \tilde{p}_{\text{off}}(k; M)]. \quad (14)$$

Here, we consider that the photo- z blurring just decreases the overall amplitude of $w(R)$ (or the Fourier-transform $C_{gg}(k)$) without changing the shape. The parameter $\Delta\chi$ represents the distance corresponding to the photo- z scatter. The function $\tilde{u}_{\text{NFW}}(k; M)$ is the Fourier transform of the projected NFW profile $u_{\text{NFW}}(R; M)$ normalized with the mass M . The analytical formula of $u_{\text{NFW}}(R; M)$ is given by Wright & Brainerd (2000). The parameter q_{cen} is the fraction of galaxies in the sample that are located at the halo centre. The function \tilde{p}_{off} is the Fourier transform of the radial profile of off-centred galaxies, hereafter referred to as the off-centred profile. The radial profile of red galaxies around galaxies that are not central galaxies are flattened depending on the off-centred profile. We adopt two models to describe the off-centred profile of galaxies. One is the Gaussian offset model, i.e., $\tilde{p}_{\text{off}}(k; M) = \exp(-k^2 R_{\text{off}}^2(M)/2)$ (e.g., Oguri & Takada 2011). The scale of this offset is defined as a fixed fraction of the halo radius as: $R_{\text{off}}(M) = \tau_{\text{off}} r_{200}(M)$ where τ_{off} is left as a free parameter. The other is the NFW offset model, i.e., $\tilde{p}_{\text{off}}(k; M) = \tilde{u}_{\text{NFW}}(k; M)$ where the concentration parameter is proportional to the halo concentration as $c_{\text{off}} c(M)$ and c_{off} is left as a free parameter. When estimating the mean halo mass via Equation 6, we integrate over the halo mass distribution of the sample, $P(M)$. Since the redshift evolution for $P(M)$ is small during the current redshift range as discussed in Simet et al. (2017), we do not include redshift evolution and assume a single mean redshift of 0.25. To model the cross-correlation functions, we limit our fits to $0.1h^{-1}\text{Mpc} < R < 2h^{-1}\text{Mpc}$, where contributions from the two-halo term are negligible.

In addition, we also compare our off-centring models with galaxy-galaxy lensing measurements. The galaxy-galaxy lensing is estimated using the excess surface mass density

$$\Delta\Sigma(R) \equiv \int \frac{k dk}{2\pi} C_{\Sigma g}(k) J_2(kR), \quad (15)$$

where $C_{\Sigma g}(k)$ is the galaxy-lensing cross-power spectrum

$$C_{\Sigma g}(k) = \int dM P(M) M \tilde{u}_{\text{NFW}}(k; M) \times [q_{\text{cen}} + (1 - q_{\text{cen}}) \tilde{p}_{\text{off}}(k; R_{\text{off}}(M))] + M_{\text{sub}}. \quad (16)$$

The last term represents the subhalo/baryonic core component approximated as a stellar mass of M_* , which is set to be $\log(M_*/h^{-1}M_{\odot}) = 11.4$ (e.g., Leauthaud et al. 2016).

5 RESULTS

We perform a simultaneous fit to the cross-correlation measurements of the three samples (High Pcen, RMCG, and BMEM) using Equation 13. There are 7 free parameters in our model listed in Table 1. Two of these parameters are common for all these samples: the photo- z scatter $\Delta\chi$ and the amplitude of the mass-concentration relation c_{amp} . There are then five free parameters: the central fractions of RMCG and BMEM samples $q_{\text{cen}}^{\text{RMCG/BMEM}}$ and the off-centring scales for High Pcen, RMCG, and BMEM samples: off-centring scale relative to the halo size $\tau_{\text{off}}^{\text{HighPcen/RMCG/BMEM}}$ in the Gaussian offset model; concentration parameter in the off-centring profile relative to the halo concentration parameter $c_{\text{off}}^{\text{HighPcen/RMCG/BMEM}}$ in the NFW offset model.

In this work, we assume that the High Pcen sample selects a high fraction of central galaxies. For this sample, we therefore put a strong prior on the central fraction $q_{\text{cen}}^{\text{HighPcen}} = [0.95, 1]$, while the central fractions for other samples are allowed to vary in the entire range $q_{\text{cen}}^{\text{RMCG/BMEM}} = [0, 1]$. We also add a loose prior $\tau_{\text{off}} = [0, 1]$ for all three samples and $c_{\text{off}} = [0, 10]$. Finally, we require that the sum of the central fractions for RMCG and BMEM samples does not exceed unity, that is, $q_{\text{cen}}^{\text{RMCG}} + q_{\text{cen}}^{\text{BMEM}} \leq 1$.

Figure 2 shows the comparison of the observed cross-correlation measurements for our best-fitting model. Our simple model using NFW profiles provides an excellent description of the cross-correlation measurements. The minimum chi-squared value χ_{min}^2 is 16.3 for d.o.f= 37 (45 data points minus 8 parameters) where the error is estimated by jackknife resampling and the covariance among the samples at each bin of R is included. One can see that the central fraction for the RMCG sample is much larger than the BMEM sample, which is consistent with the values reported by redMaPPer.

As a consistency check, we also compare the galaxy-galaxy lensing measurements $\Delta\Sigma$ with the prediction of the theoretical model (Eq. 15). We use the best-fitting values of q_{cen} and τ_{off} obtained from the cross-correlation measurements. We do not use $\Delta\chi$ and c_{amp} parameters as they are only relevant for the clustering cross-correlation measurement and not for the underlying matter distribution probed by the cluster-galaxy lensing. As shown in Figure 3, we find that the lensing measurements are consistent with our theoretical model. The χ^2 values are 27.5 for the 24 data points, while for the High Pcen sample, the χ^2 value is 7.2 for 8 data points.

Figure 4 shows the constraints on our parameters from the cross-correlation measurements w_{gg} . Red solid lines show the mean values reported by redMaPPer for $(q_{\text{cen}}^{\text{RMCG}}, q_{\text{cen}}^{\text{BMEM}})$. These are consistent with our constraint obtained from the cross-correlation measurements within 1σ . Tables 2 and 3 list the marginalized constraints on each parameter. Our constraint on the central fraction is 0.74 ± 0.09 for RMCG samples and 0.13 ± 0.04 for BMEM samples, consistent with the redMaPPer mean values of 0.754 and 0.103, respectively. The average values of $r_{200}(M)$ are $1.1h^{-1}\text{Mpc}$ for the three samples. The physical off-centring scale converted from the fitted τ_{off} values is $0.2\text{--}0.3h^{-1}\text{Mpc}$ consistently across the three samples. The error on the off-centring scale for “High Pcen” is large since the off-centring fraction is so low. When adopting the NFW offset model, the constraints on the central fraction becomes 0.77 ± 0.09 for RMCG samples and 0.05 ± 0.05 for BMEM samples, which is also consistent with the redMaPPer estimates.

We note that our results rely on the prior that the High Pcen

Parameter	Description
$\Delta\chi[h^{-1}\text{Mpc}]$	Distance corresponding to photo- z scatter
c_{amp}	Amplitude of mass-concentration relation
$q_{\text{cen}}^{\text{RMCG}}$	Fraction of central galaxies in RMCG sample
$q_{\text{cen}}^{\text{BMEM}}$	Fraction of central galaxies in BMEM sample
$\tau_{\text{off}}^{\text{HighPcen}}$	Ratio of off-centring scale to $r_{200}(M)$ in High Pcen sample in Gaussian offset model
$\tau_{\text{off}}^{\text{RMCG}}$	Ratio of off-centring scale to $r_{200}(M)$ in RMCG sample in Gaussian offset model
$\tau_{\text{off}}^{\text{BMEM}}$	Ratio of off-centring scale to $r_{200}(M)$ in BMEM sample in Gaussian offset model
$c_{\text{off}}^{\text{HighPcen}}$	Ratio of concentration parameter to $c(M)$ in High Pcen sample in NFW offset model
$c_{\text{off}}^{\text{RMCG}}$	Ratio of concentration parameter to $c(M)$ in RMCG sample in NFW offset model
$c_{\text{off}}^{\text{BMEM}}$	Ratio of concentration parameter to $c(M)$ in BMEM sample in NFW offset model

Table 1. Free parameters in our modeling and their short descriptions.

$\Delta\chi[h^{-1}\text{Mpc}]$	c_{amp}	$q_{\text{cen}}^{\text{HighPcen}}$	$q_{\text{cen}}^{\text{RMCG}}$	$q_{\text{cen}}^{\text{BMEM}}$	$\tau_{\text{off}}^{\text{HighPcen}}$	$\tau_{\text{off}}^{\text{RMCG}}$	$\tau_{\text{off}}^{\text{BMEM}}$
200 ± 3	1.06 ± 0.06	0.98 ± 0.01	0.74 ± 0.10	0.13 ± 0.04	0.38 ± 0.25	0.20 ± 0.06	0.31 ± 0.01

Table 2. $1-\sigma$ marginalized constraint on each parameter obtained by joint fitting of $w(R)$ for the High Pcen, redMaPPer central galaxy (RMCG), and the brightest member galaxy (BMEM) samples. The fitted parameters are 8 in total: the photo- z scatter $\Delta\chi$ and concentration c_{amp} , which are common for the three samples, and the central fraction q_{cen} and the relative offset τ_{off} for three samples. We put the strong prior on the central fraction for High Pcen sample $q_{\text{cen}}^{\text{HighPcen}} = [0.95, 1]$. The fitted range of scale from $0.1h^{-1}\text{Mpc}$ to $2h^{-1}\text{Mpc}$ and the covariance among different samples in each bin in R is taken into account.

sample has a nearly true radial profile of photo- z red galaxies without off-centring, i.e., $q_{\text{cen}}^{\text{HighPcen}} = [0.95, 1]$. Since the galaxies in the High Pcen sample usually have well-defined central galaxies, the prior is reasonable. The posterior distribution of $q_{\text{cen}}^{\text{HighPcen}}$ however has a peak at 0.95, the minimum edge of our prior. This may indicate that our modeling does not perfectly describe the observed galaxy radial profile for several reasons (e.g., baryonic feedback effect). Nevertheless, our results for the off-centring values are determined by the difference ratio of the radial profiles among the samples. As long as the High Pcen sample has a true galaxy radial profile, the off-centring values for the other samples are barely affected by the details in the modeling of the radial profile.

6 SUMMARY

We have investigated whether photometrically derived redMaPPer centring probabilities are valid for the cluster sample in which the brightest member galaxy (BMEM) is not the redMaPPer central galaxy (RMCG), that is, the galaxy with the highest centring probability in each cluster. We measure the projected cross correlation function of each cluster ‘centre’ with photometric red galaxies, which is sensitive to the off-centring fraction. We use ‘‘High Pcen’’ sample where the RM centring probabilities is larger than 99% as a reference sample of central galaxies. We find that the centring fraction is $74 \pm 10\%$ for RMCGs and $13 \pm 4\%$ for BMEM when the radial profile of off-centred galaxies follows a Gaussian form. When adopting the NFW model for the off-centred profile, the constraints on the centring fraction becomes $78 \pm 9\%$ for RMCGs and $5 \pm 5\%$ for BMEM. The values are consistent with the redMaPPer values, 75% for RMCG and 10% for BMEM. Our analysis is a strong self-consistency test of the RM centring probabilities. Our results indicate that the redMaPPer centroids are better tracers of the centre of the cluster potential than the brightest cluster mem-

bers, and that the redMaPPer algorithm provides accurate estimates of centring probabilities for the proposed cluster centres.

We also measure galaxy-galaxy lensing to find that the measurements are consistent with our lensing models with the best-fitting off-centring values obtained from the cross-correlation measurements. The statistical error is much larger than that of the cross-correlation measurements because of the large shot noise due to the limited number of source galaxies. The lensing signal will be substantially improved by using upcoming deeper imaging surveys such as Subaru Hyper-Suprime Cam and Dark Energy Survey, which have a much higher number density of source galaxies than SDSS, enough to compensate for their smaller areas.

We show that the redMaPPer centring algorithm provides reliable estimates of centring probabilities using the cross-correlation measurements. This is consistent with the previous work by Rozo & Rykoff (2014) who studied the centring probability by comparison with X-ray clusters. Our result supports the work by Hoshino et al. (2015) who investigated the central occupation of LRGs and BMEMs based on the redMaPPer centring probabilities. They found that 20~30% of redMaPPer clusters the brightest cluster member galaxies are not central galaxies. The redMaPPer centring algorithm is also useful for calibrating off-centring effect in various studies such as mass estimates using stacked lensing analysis (Johnston et al. 2007; Leauthaud et al. 2010; Okabe et al. 2010; Oguri & Takada 2011; George et al. 2012; Oguri et al. 2017). RSD studies using reconstructed ‘‘halo’’ catalogs have the uncertainty of the off-centring fraction (Hikage et al. 2012), which can be mitigated using the redMaPPer centring values.

ACKNOWLEDGMENTS

CH is supported by MEXT/JSPS KAKENHI Grant Numbers 16K17684. RM is supported by the Department of Energy Early Career Award program.

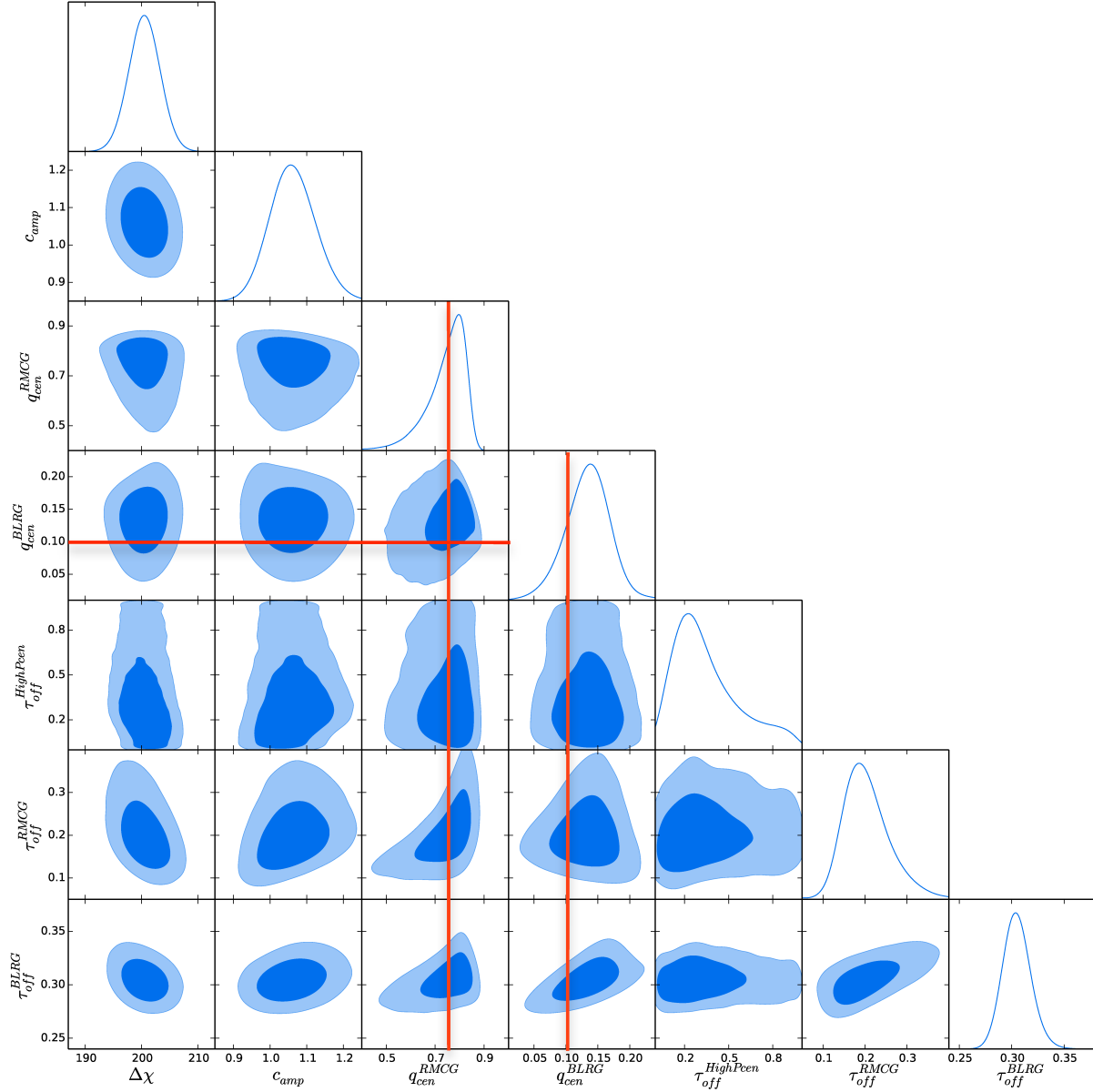


Figure 4. $1\text{-}\sigma$ and $2\text{-}\sigma$ constraints on the parameters obtained from the cross-correlation measurements $w(R)$ in the three samples. The distribution in the diagonal panels shows the posterior distribution of each parameter after marginalizing over the other parameters. The red solid lines represent the redMaPPer values of mean central fractions for the RMCG and BMEM samples. As shown, the model fits to cross-correlation data give consistent off-centring fractions with those inferred from the redMaPPer centring probabilities.

$\Delta\chi[h^{-1}\text{Mpc}]$	c_{amp}	$q_{\text{cen}}^{\text{HighPcen}}$	$q_{\text{cen}}^{\text{RMCG}}$	$q_{\text{cen}}^{\text{BMEM}}$	$c_{\text{off}}^{\text{HighPcen}}$	$c_{\text{off}}^{\text{RMCG}}$	$c_{\text{off}}^{\text{BMEM}}$
200 ± 3	1.06 ± 0.06	0.97 ± 0.01	0.78 ± 0.09	0.05 ± 0.05	5.1 ± 2.8	5.2 ± 2.8	0.88 ± 0.20

Table 3. Same as Table 2, but the results in the NFW offset model. The parameters related to off-centring scales τ_{off} are replaced by c_{off} .

REFERENCES

- Aihara H. et al., 2011, ApJS, 193, 29
 Alam S. et al., 2015, ApJS, 219, 12
 Berlind A. A., Weinberg D. H., 2002, ApJ, 575, 587
 Budzynski J. M., Kopolov S. E., McCarthy I. G., McGee S. L.,
 Belokurov V., 2012, MNRAS, 423, 104
 Cabré A., Gaztañaga E., 2009, MNRAS, 393, 1183
 Coupon J. et al., 2012, A.&Ap., 542, A5
 Coziol R., Andernach H., Caretta C. A., Alamo-Martínez K. A.,
 Tago E., 2009, AJ, 137, 4795
 Dawson K. S. et al., 2013, AJ, 145, 10

- Diemer B., Kravtsov A. V., 2015, *ApJ*, 799, 108
- Einasto M. et al., 2011, *ApJ*, 736, 51
- Feldmann R. et al., 2006, *MNRAS*, 372, 565
- George M. R. et al., 2012, *ApJ*, 757, 2
- Guo H. et al., 2015, *MNRAS*, 453, 4368
- Hansen S. M., Sheldon E. S., Wechsler R. H., Koester B. P., 2009, *ApJ*, 699, 1333
- Hikage C., Mandelbaum R., Takada M., Spergel D. N., 2013, *MNRAS*, 435, 2345
- Hikage C., Takada M., Spergel D. N., 2012, *MNRAS*, 419, 3457
- Hikage C., Yamamoto K., 2013, *JCAP*, 8, 019
- Hirata C., Seljak U., 2003, *MNRAS*, 343, 459
- Ho S., Lin Y.-T., Spergel D., Hirata C. M., 2009, *ApJ*, 697, 1358
- Hoshino H. et al., 2015, *MNRAS*, 452, 998
- Ivezic Z. et al., 2008, *ArXiv e-prints arXiv:0805.2366*
- Johnston D. E. et al., 2007, *ArXiv e-prints arXiv:0709.1159*
- Lauer T. R., Postman M., Strauss M. A., Graves G. J., Chisari N. E., 2014, *ApJ*, 797, 82
- Leauthaud A. et al., 2016, *MNRAS*, 457, 4021
- Leauthaud A. et al., 2010, *ApJ*, 709, 97
- Leauthaud A., Tinker J., Behroozi P. S., Busha M. T., Wechsler R. H., 2011, *ApJ*, 738, 45
- Mahdavi A., Hoekstra H., Babul A., Bildfell C., Jeltema T., Henry J. P., 2013, *ApJ*, 767, 116
- Mandelbaum R., Hirata C. M., Leauthaud A., Massey R. J., Rhodes J., 2012, *MNRAS*, 420, 1518
- Mandelbaum R. et al., 2005, *MNRAS*, 361, 1287
- Mandelbaum R., Seljak U., Kauffmann G., Hirata C. M., Brinkmann J., 2006, *MNRAS*, 368, 715
- Mandelbaum R., Slosar A., Baldauf T., Seljak U., Hirata C. M., Nakajima R., Reyes R., Smith R. E., 2013, *MNRAS*, 432, 1544
- Manera M. et al., 2013, *MNRAS*, 428, 1036
- Masjedi M. et al., 2006, *ApJ*, 644, 54
- Menanteau F. et al., 2013, *ApJ*, 765, 67
- Miyazaki S. et al., 2012, in *SPIE*, Vol. 8446, *Ground-based and Airborne Instrumentation for Astronomy IV*, p. 84460Z
- Nakajima R., Mandelbaum R., Seljak U., Cohn J. D., Reyes R., Cool R., 2012, *MNRAS*, 420, 3240
- Navarro J. F., Frenk C. S., White S. D. M., 1996, *ApJ*, 462, 563
- Oguri M., 2014, *MNRAS*, 444, 147
- Oguri M. et al., 2017, *ArXiv e-prints arXiv:1701.00818*
- Oguri M., Takada M., 2011, *Phys. Rev. D*, 83, 023008
- Okabe N., Takada M., Umetsu K., Futamase T., Smith G. P., 2010, *PASJ*, 62, 811
- Parejko J. K. et al., 2013, *MNRAS*, 429, 98
- Reid B. A., Spergel D. N., 2009, *ApJ*, 698, 143
- Reid B. A., Spergel D. N., Bode P., 2009, *ApJ*, 702, 249
- Reyes R., Mandelbaum R., Gunn J. E., Nakajima R., Seljak U., Hirata C. M., 2012, *MNRAS*, 425, 2610
- Rozo E., Rykoff E. S., 2014, *ApJ*, 783, 80
- Rozo E., Rykoff E. S., Becker M., Reddick R. M., Wechsler R. H., 2015, *MNRAS*, 453, 38
- Rykoff E. S. et al., 2014, *ApJ*, 785, 104
- Samushia L., Percival W. J., Raccanelli A., 2012, *MNRAS*, 420, 2102
- Sanderson A. J. R., Edge A. C., Smith G. P., 2009, *MNRAS*, 398, 1698
- Scoccimarro R., Sheth R. K., Hui L., Jain B., 2001, *ApJ*, 546, 20
- Sehgal N. et al., 2013, *ApJ*, 767, 38
- Seljak U., 2000, *MNRAS*, 318, 203
- Sheldon E. S. et al., 2009, *ApJ*, 703, 2217
- Simet M., McClintock T., Mandelbaum R., Rozo E., Rykoff E., Sheldon E., Wechsler R. H., 2017, *MNRAS*, 466, 3103
- Singh S., Mandelbaum R., Seljak U., Slosar A., Vazquez Gonzalez J., 2017, *MNRAS*, 471, 3827
- Skibba R. A., 2009, *MNRAS*, 392, 1467
- Skibba R. A., van den Bosch F. C., Yang X., More S., Mo H., Fontanot F., 2011, *MNRAS*, 410, 417
- Stott J. P. et al., 2012, *MNRAS*, 422, 2213
- The Dark Energy Survey Collaboration, 2005, *ArXiv Astrophysics e-prints astro-ph/0510346*
- van den Bosch F. C., Aquino D., Yang X., Mo H. J., Pasquali A., McIntosh D. H., Weinmann S. M., Kang X., 2008, *MNRAS*, 387, 79
- van den Bosch F. C., Norberg P., Mo H. J., Yang X., 2004, *MNRAS*, 352, 1302
- van den Bosch F. C., Weinmann S. M., Yang X., Mo H. J., Li C., Jing Y. P., 2005, *MNRAS*, 361, 1203
- von der Linden A. et al., 2014, *MNRAS*, 439, 2
- von der Linden A., Best P. N., Kauffmann G., White S. D. M., 2007, *MNRAS*, 379, 867
- Weinmann S. M., van den Bosch F. C., Yang X., Mo H. J., 2006, *MNRAS*, 366, 2
- White M. et al., 2011, *ApJ*, 728, 126
- Wright C. O., Brainerd T. G., 2000, *ApJ*, 534, 34
- York D. G. et al., 2000, *AJ*, 120, 1579
- Zheng Z., et al., 2005, *ApJ*, 633, 791